The 2009 IEEE/RSJ International Conference on
Intelligent Robots and Systems
October 11-15, 2009 St. Louis, USA

Enhanced haptic device compatible with fMRI environment

Ales Hribar, Blaz Koritnik and Marko Munih

Abstract— **Paper presents an upgrade of a Phantom Premium 1.5 haptic device for use within a functional magnetic resonance imaging (fMRI) environment. A mechanical extension attached to the Phantom allows the haptic device to operate at a safe distance away from a high-density magnetic field of an fMRI scanner. The extended haptic system was subjected to a series of tests to confirm electromagnetic compatibility with the fMRI environment, for which key results are presented. With the extended fMRI compatible haptic platform a human brain activation during controlled upper limb movements can be studied. A virtual environment reaching task was programmed to study brain motor control functions. At the end of the paper a preliminary results of an ongoing neurophysiological study are presented.**

I. Introduction

Magnetic resonance imaging (MRI) is a standard non-invasive tool used in clinical diagnostics and research into the human body. Over the past few years, functional MRI (fMRI) has established itself as a curtail method in human brain research. The fMRI technique is based on the measurement of blood oxygen level-dependent (BOLD) signals for estimation of neural activity in the brain [1]. Clinical studies [2], [3] have investigated human brain activation during voluntary upper-limb movements. However, a controlled movement task could provide new insights into human motor control. To asses and control isotonic, isometric or any other form of arm activity, a device capable of generating and measuring forces and trajectories is needed. A haptic device is suitable for these and a span of other combined activities that depend on position, velocity and acceleration. To perform such tasks inside an fMRI scanner, an fMRI compatible haptic interface is required.

A device used inside an fMRI environment requires a high level of safety and electromagnetic compatibility [4]. There are several difficulties that impose limits on the use of electromechanical devices inside fMRI scanners. The high magnetic flux density makes the use of ferromagnetic materials impossible (missile effect). The high-level radio-frequency electromagnetic field and the sensitivity of the scanner receiver coils limit the use of electronic circuits. With a typical diameter of 60 cm, there is also limited space within the scanner bore. These limitations make the design of an fMRI compatible device a challenging task.

This work was supported by Slovenian Research Agency (ARRS)

Ales Hribar is with Faculty of Electrical Engineering, University of Ljubljana, Slovenia alesh@robo.fe.uni-lj.si

Blaz Koritnik is with University Medical Centre Ljubljana, Division of Neurology, Institute of Clinical Neurophysiology, Slovenia blaz.koritnik@kclj.si

Marko Munih is with Faculty of Electrical Engineering, University of Ljubljana, Slovenia marko@robo.fe.uni-lj.si

Nevertheless, scientists working in the field of human motor control require a tool capable of dynamically controlling arm and hand movements inside an fMRI scanner. Recently a few such devices have been developed. fMRI compatible hand rehabilitation devices were introduced by Khanicheh et al. [5], [6]. Simple 1-DOF haptic interfaces have also been reported [7], [8], [9], [10]. More sophisticated haptic devices have been described [11], [12], one of which has 2-DOF and uses hydraulic actuators to generate force [11]. Another 2-DOF haptic device is powered by an ultrasonic motor [12].

However, to the best to our knowledge, no 3-DOF haptic interface has been introduced to an fMRI environment to date. An important issue in fMRI experiments is the ability to imitate reality as closely as possible inside the scanner. A three-dimensional virtual environment represents a good approach. This motivated us to upgrade the Phantom Premium 1.5 haptic device to work inside an fMRI scanner room. Employing this widely accepted haptic device enabled us to use the existing software, thus accelerating design of the system. A mechanical carbon-fiber extension with a 3-DOF joint has been developed and coupled to the end-effector of the Phantom haptic device. This ensures that the Phantom can operate at a safe distance, well outside the high magnetic field of the main coil of the fMRI scanner.

II. Methods and Materials

A. Phantom Premium 1.5

Phantom Premium 1.5 (SensAble Technologies, Inc., Woburn, MA) is a commercially available 3-DOF haptic device. It has already been used in our laboratory to study upper limb movements [14]. This was the main reason to use this, among research community, widely accepted haptic device. We were also trying to incorporate as much of the developed software as possible.

The Phantom has an adequate workspace of 381 mm $\times$ 267 mm $\times$ 191 mm and maximum exertable force of 8.5 N [15]. It's small size and light weight enabled us to quickly mount it on and off the support structure used in fMRI experiment.

B. Haptic system

The Phantom is driven by electric coreless motors. For a small electric motor operating inside the fMRI examination room, the maximum permitted magnetic flux density generated by the scanner is 3 mT [16]. Data supplied by Siemens suggested that the Phantom would have to be at a distance of 3 m away from the center of the magnet to meet this requirement. Additional measurements of the magnetic flux density were carried out to determine the exact position for

the Phantom inside the scanner room. These measurements confirmed that the Phantom would need to be coupled using a 2 m long extension between the end-effector of the Phantom and the subject's hand to satisfy the maximum magnetic flux density.

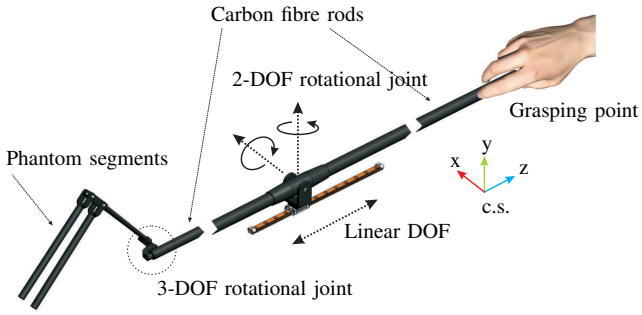

Fig. 1. Mechanical extension with a 3-DOF joint in the middle. Note that only parts of the carbon fiber rods are shown.

The mechanical extension shown in Figure 1 comprises two carbon fiber rods, a 2-DOF gimbal, and a linear rail with a carriage. An aluminum part with an $M22\times$ 1.5 thread is glued to the end of each carbon fiber rod. The rods are screwed into a gimbal cylinder, which is mounted on a main gimbal frame using a bronze axle and Teflon bearings. The main gimbal frame rotates on the bronze axle mounted on the rail carriage. Non-ferromagnetic stainless steel hex screws are used to secure both axles. Final assembly gives the mechanical extension 3-DOF. The linear rail with the carriage provides a translational DOF and the gimbal adds two rotational DOF.

The stainless steel rail and the RSR9ZM carriage were purchased from THK (THK Company Ltd., Tokyo, Japan). The 2-DOF aluminum gimbal was designed in Autodesk Inventor (Autodesk, Inc., San Rafael, CA) and fabricated in a CNC machine shop.

One end of the mechanical extension is coupled to the Phantom haptic device. A 3-DOF rotational joint is used to connect Phantom and the extension, which are fixed on an aluminium frame that is assembled out of Bosch Rexroth (Bosch Rexroth AG, Lohr, Germany) aluminium strut profiles. The aluminum frame is bolted together with non-ferromagnetic stainless steel screws. A special plastic part was fabricated to connect the sliding examination table of the fMRI scanner and the aluminum frame. The assembly is shown in Fig. 2.

Phantom's electric motors and encoders are connected to a controller located outside examination room through two separate LIYCY shielded cables. No additional filtering is provided.

The virtual environment in which a human subject performs the desired arm movement task comprises haptic and visual parts. The Phantom device coupled to the mechanical extension enables the subject to execute the haptic part of the task. To ensure visual feedback, a projector and a

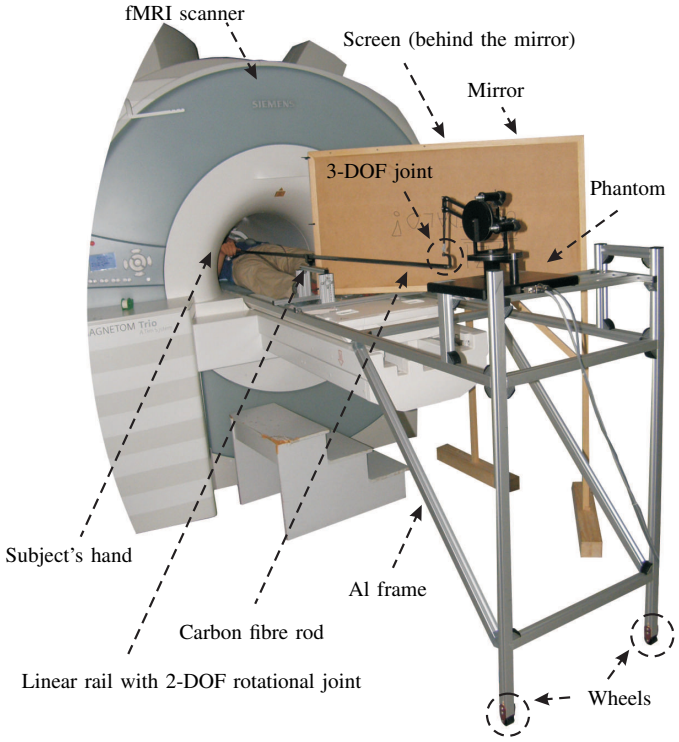

Fig. 2. Phantom haptic device coupled to the mechanical extension inside an fMRI scanner room. Haptic system is mounted on the aluminum construction.

projection screen were used. The beam of light coming from the projector enters the scanner room through a window. It is then reflected from the mirror and back-projected to the projection screen.

C. Kinematic model

With the extension added to the Phantom haptic device, original kinematic map is changed. The extension adds transformation described by eq. (1), where **pe** is positional vector in the new extended coordinate system (marked in Fig. 1) with respect to the Phantom's original coordinate system. This positional transformation added by the extension is corrected in software.

$$\mathbf{pe} = \begin{bmatrix} \mathrm{pe}_x \\ \mathrm{pe}_y \\ \mathrm{pe}_z \end{bmatrix} = \begin{bmatrix} -\mathrm{pw}_x \\ -\mathrm{pw}_y \\ \mathrm{pw}_z - 2\sqrt{l^2 - {\mathrm{pw}_x}^2 - {\mathrm{pw}_y}^2} \end{bmatrix} \quad (1)$$

D. Experimental software

Software was developed using Microsoft Visual studio. The graphic part of application was programmed using the OpenGL graphic library. A haptic environment was created using a GHOST 4.0 software development kit. GHOST SDK (General Haptic Open Software Toolkit) is a C++ software toolkit that simplifies the development of haptic environment applications. High-level objects and physical properties can be created in a few lines of code. The GHOST SDK "physics of touch" engine carries out the complex

computations required. The rendering frequency of the main haptic loop is 1 kHz.

Our goal was to develop haptic and visual virtual-environment task whereby a human subject would perform reaching movements. The simple virtual-environment room shown in Fig. 3 was created for performance of the task. The haptic dimensions of the room are 140 mm $\times$ 100 mm $\times$ 80 mm. The position of a white cursor ball in the virtual environment room reflects the position of the end-effector point of the coupled haptic system. The virtual environment session comprised four tasks: rest before reaching (RR), target reaching (R), rest before extension (RE) and non-targeting arm extension (E).

In the first task (RR), the edges of the virtual environment room are colored red, indicating that the subject should just observe the room and not perform any arm movements. In the upper right quadrant on the back wall of the room, a white square target is shown for 1 s at a randomly generated position. The time interval before the next target is shown is pseudo-randomly selected from the interval between 4 and 6 s so that the duration of the whole task (six trials) is 30 s.

In next task (R), the edges of the room turn green. The subject must now move the white cursor ball to the middle of the edge formed by the bottom and front walls and wait for the target. Then a white square target is shown and the subject is instructed to hit the target with the cursor as fast and as accurately as possible. When hit, the target disappears and the subject must move the cursor to the start position. Six reaching trials are performed during task R. The target size, timing and positioning are the same as in the previous RR task.

Red edges of the room in the RE task indicate subject rest. A large square with a white border is displayed on the back wall. The room with the square is shown in Fig. 3(a). The time sequence for display of the square is the same as in the RR task. The square is always at the same position in the first quadrant of the back wall.

The last trial begins when the edges of the room turn green. As soon as the large square is displayed, the subject must move the cursor anywhere inside the white border, representing non-targeting arm extension. When the inside of the square is hit, the square disappears. The position, timing and size of the square target are the same as in the RE task.

A complete virtual-environment session consists of eight blocks, each containing four of the above-mentioned tasks. The duration of each block is 2 min, with 30 s for each task in the block.

A log file is created for every run of the virtual environment session. Each line of the log file comprises 11 parameters: time from the beginning of the session, x, y, and z positions, and x, y, and z forces of the Phantom end-effector. "Show target", "Start", and "Hit target" are the three flags written to the log file. A synchronization signal produced by the fMRI scanner is read through the LPT and written to the log file as the final parameter. This synchronization signal is important in synchronizing fMRI images and data from the log file during data analysis. The

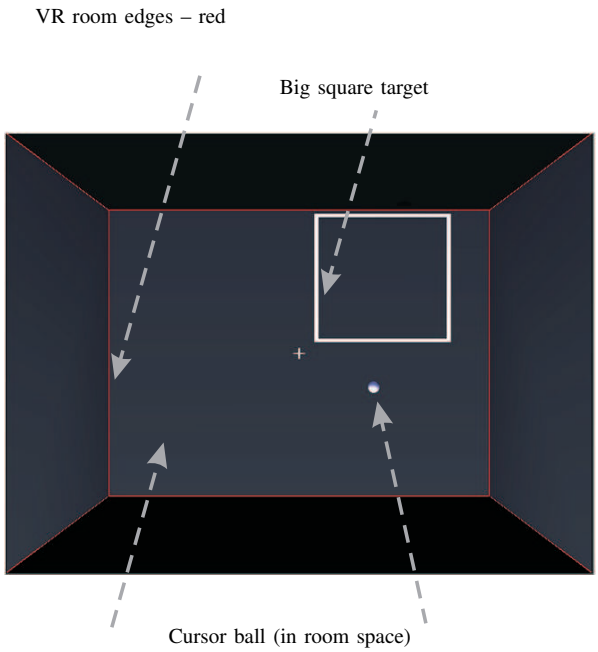

(a) Rest before extension

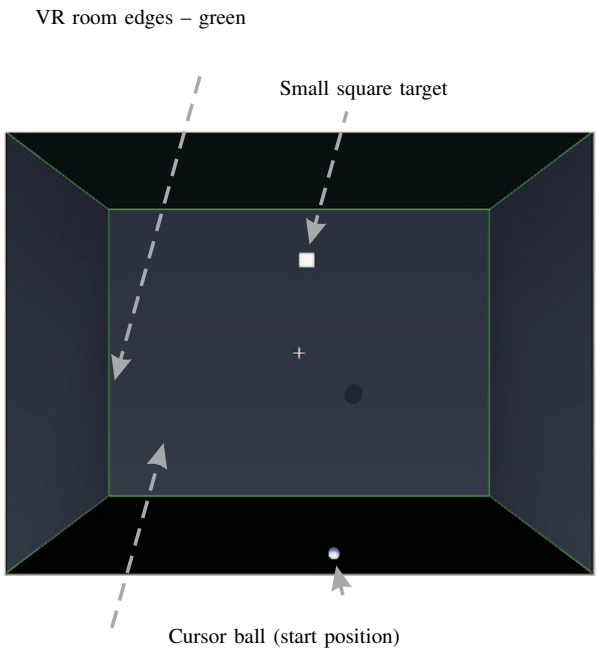

(b) Reaching

Fig. 3. Virtual environment room during different trials.

period of the signal T_R was 3 s.

E. Evaluation experiment

First experiment with the Phantom coupled to the mechanical extension was carried out in a controlled environment

outside the fMRI scanner. Aim of this experiment was to asses the impact of the mechanical extension on a subject performance during execution of a virtual environment task. A virtual environment task was programmed where the subject had to reach for a white square target on a back wall of a virtual environment room.

The experiment comprised two parts. Each of five male volunteers (age range 26–29 years) first executed the virtual environment task using only the Phantom haptic device. In the second part of the experiment, the mechanical extension was added to the Phantom and the same task was repeated. A log file containing trajectories, forces, start and hit times for each subject was generated for every run. Data from these two experimental sets allowed us to study the effect of the mechanical extension on the trajectories, velocities and forces and the reaction times of the subject while performing the virtual environment task.

F. Electromagnetic compatibility

To investigate the electromagnetic compatibility of the extended haptic system, a series of tests were carried out. First, we observed the effect of the fMRI scanner on the extended haptic system. Extended haptic system was installed in the the fMRI examination room. The Phantom was connected to the controller and the virtual environment task was started. Meanwhile a echo planar (EPI) fMRI sequence with T_R = 3000 ms, T_E = 30 ms, FOV = 192 mm, 36 slices, 6 mm slice thickness, 3x3x3 mm^3 voxel size was ran on the fMRI scanner. Any possible disturbance in the Phantom's operation has been observed.

Next step was to examine the influence of operation of the extended haptic system on the fMRI scanner. A cylindrical phantom object – not to be confused with the Phantom haptic device – (plastic bottle 1900 ml, per 1000 g H_2O dist.: 3.75 g $NiSO_4$ x $6H_2O$ + 5 g NaCl) was placed inside the fMRI scanner in the place where the subject's head usually lies. With no haptic device present inside the examination room a set of reference fMRI images was acquired. Then the extended haptic device was placed inside the examination room and two more sets were acquired. First set with the Phantom turned off and second set with the virtual environment task active. A volunteer inside the fMRI examination room, but outside the scanner was manipulating with the extended haptic device while acquiring second set of images. The fMRI sequence parameters were fixed throughout all three phases of the test and were the same as in the experiment described in the previous paragraph.

Signal to noise ratios (SNR) for two sets of acquired images were calculated according to [17].

G. fMRI experiment

A 15 min training session in which subject got used to the system was ran before the fMRI trial. The subject exercised with the same virtual environment task as later in the trial. During the fMRI experiment functional images were acquired using EPI fMRI sequence described earlier. The total scanning time was 6 min and 320 whole-brain functional images were acquired. All of the image analysis, including realignment, normalization, smoothing and statistical analysis based on a general linear model [18], was performed using Statistical Parametrical Mapping implemented in MATLAB (The MathWorks, Inc., Natick, MA). The four tasks (see above) were modeled as box car functions convolved with the hemodynamic response functions. After estimation of all model parameters, differences between the tasks were assessed by applying the following linear contrasts to the parameter estimates: R–RR, E–RE and R–E. A voxel threshold of $P < 0.05$ (corrected for multiple comparisons) was used for R–RR and E–RE, whereas an uncorrected threshold of $P < 0.001$ was used for the R–E comparison.

All experiments presented in this paper were carried out on a Siemens Trio 3 T (Siemens Healthcare, Erlangen, Germany) fMRI scanner.

III. Results

A. Evaluation experiment

A comparison of reaching trajectories with and without the extension is presented in Fig. 4(a). Each trace represents an average of 20 trajectories captured from one subject. For demonstration purposes and clarity, only one coordinate is presented.

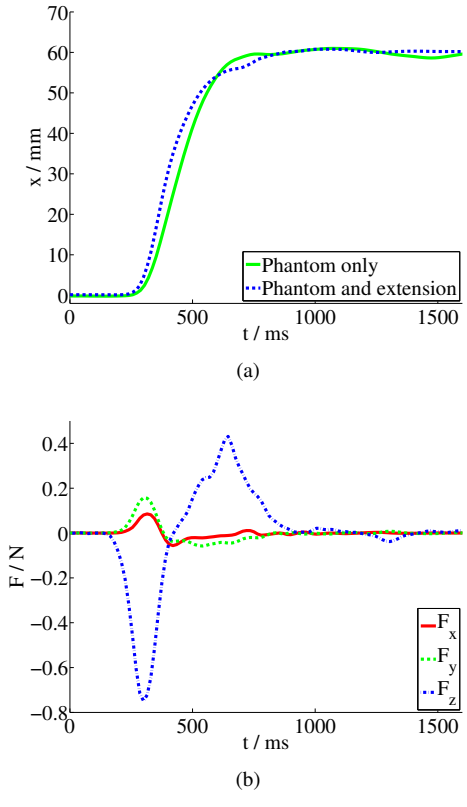

Fig. 4. (a) Comparison of trajectories with (dashed line) and without (full line) the mechanical extension during evaluation of the reaching task outside the fMRI scanner. (d) Forces induced by the mechanical extension. The coordinate system is marked in Fig. 1.

The virtual environment task requires no interaction forces, when the subject moves the cursor in free space of the virtual environment room. When the Phantom is used without the extension, actual interaction forces with the subject are a result of the Phantom dynamics. The use of the extension changes these interaction forces due to the difference in the dynamic model. Forces induced by the movement of the extension are presented in Fig. 4(b).

TABLE I

REACTION AND MOVEMENT TIMES VALUES IN MS ARE GIVEN AS: MEAN (STANDARD DEVIATION)

Mode	$T_{Reaction}$	$T_{Movement}$	T_{Total}
Phantom only	310 (33)	770 (236)	1080 (248)
Haptic system	315 (36)	780 (231)	1095 (244)

Comparison of execution times during the virtual environment task. Reaction time is measured between the moment when the white square target is shown on the screen and the moment in which subject starts to move the cursor. Movement time is time in which subject is moving the cursor towards the target. Total time is sum of the movement and reaction time. Data in Table I is an average of all times of five subjects who have participated in the experiment.

B. Electromagnetic compatibility

No disturbances in the operation of the Phantom haptic device were detected in the first or in any of the following test experiments. For the first set of acquired images a SNR of 172 was calculated. SNR for the second set was 170. Acquired images did not reveal any abnormalities during visual inspection of trained personnel.

C. fMRI experiment

Comparison of reaching to the rest reaching task (R–RR) revealed activations in the left primary sensorimotor cortex (SM1), bilateral premotor cortex (PMC), inferior frontal gyrus (IFG), supplementary motor area (SMA), inferior and superior posterior parietal cortex (PPC), visual cortex, left basal ganglia (BG) and predominantly the right cerebellar hemisphere (Fig. 5(b)). During non-targeted arm extension (E–RE), similar but less prominent brain activations were found, including right SM1, bilateral PMC, IFG, SMA, inferior PPC, visual cortex and right CRB. Direct comparison of reaching to arm extension (R–E) revealed that areas showing greater activation during R were the bilateral prefrontal cortex, SMA, right visual cortex and right CRB.

IV. DISCUSSION

Maximum force induced by the extension, which appears when moving extension in z direction, has insignificant effect on subject performance during the execution of the virtual environment task. This is also confirmed by the comparison of presented reaching trajectories and reaction times (Table I).

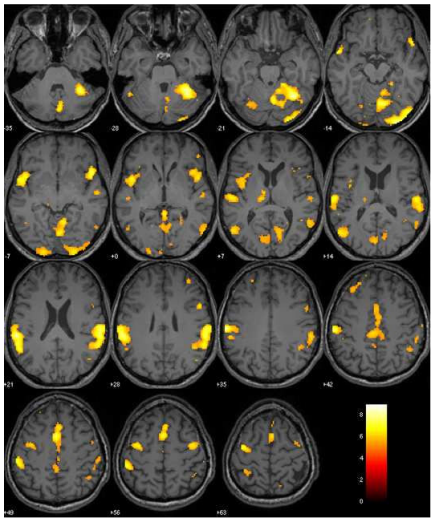

(a) Brain activation during reaching compared to rest

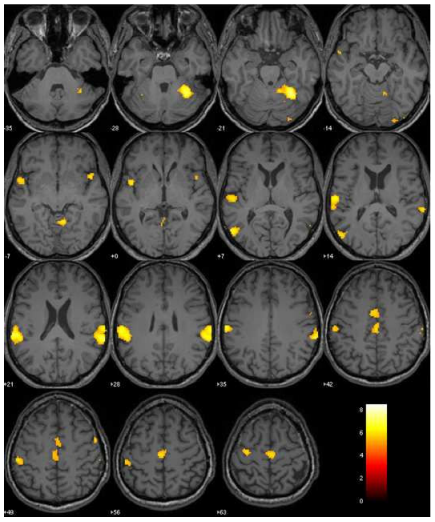

(b) Brain activation during non-targeting arm extension compared to rest

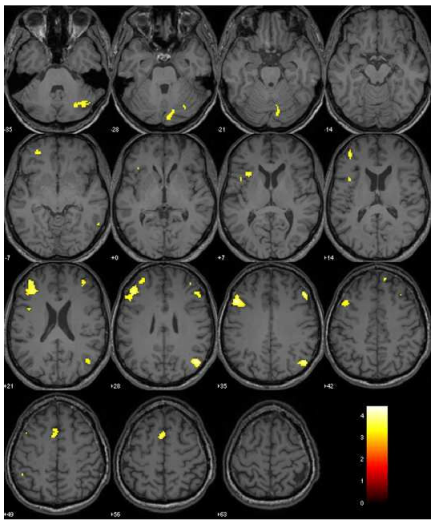

(c) Brain areas that showed greater activation during reaching compared to arm extension.

Fig. 5. fMRI maps showing brain areas activated during virtual environment tasks. Transverse slices with the right side of the brain on the right; z coordinates are shown below the slices and the color bar represents statistical t-values.

These results demonstrate that there is no notable difference in subject performance when the simple virtual environment task is executed using the Phantom device coupled to the mechanical extension, compared to execution without the extension. Results apply only to the presented virtual environment task and can not be directly generalized to other applications.

During the compatibility tests no disturbance in the operation of the Phantom haptic device or fMRI scanner were observed. Due to the fact that ferromagnetic electromechanical parts are present in the examination room, the extended haptic system can be, according to [19] , labeled as "MR-conditional".

V. Conclusions

This paper presents the upgrade and testing of a Phantom haptic device for use in fMRI environment. We were able to achieve electromagnetic compatibility of the extended haptic device without changing any of Phantom's original mechanical or electrical components. The mechanical extension and the 3-DOF joint allows the Phantom device to work outside the 3 mT magnetic flux density line that is 3 m from the isocenter of the magnet. The Phantom haptic device coupled to the mechanical extension was subjected to a series of tests that confirmed its electromagnetic and functional compatibility with the fMRI environment. A cylindrical phantom object was scanned and other measurements were utilized in fMRI compatibility tests. Tests outside the fMRI scanner also confirmed that the mechanical extension has a negligible impact on the original Phantom dynamics. We have observed a bilateral sensorimotor brain network activation during the execution of the virtual environment task. The activations were greater during the reaching task compared to arm extension. A similar fronto-parietal network for reaching has been observed in other functional neuroimaging and electrophysiological studies [20], [21], [22]. This has motivated us continue and expand the study with ten more subjects.

References

[1] Ogawa S, Menon RS, Kim SG, Ugurbil K. On the characteristics of functional magnetic resonance imaging of the brain. Annu Rev Biophys Biomol Struct 1998; 27: 447–474.

[2] Lehericy S, Bardinet E, Tremblay L, Van de Moortele PF, Pochon JB, Dormont D, Kim DS, Yelnik J, Ugurbil K. Motor control in basal ganglia circuits using fMRI and brain atlas approaches. Cerebral Cortex 2006; 16: 149–161.

[3] Toma K, Nakai T. Functional MRI in human motor control studies and clinical applications. Magn Reson Med Sci 2002; 1: 109–120.

[4] Schueler BA, Parrish TB, Lin JC, Hammer BE, Pangrle BJ, Ritenour ER, Kucharczyk J, Truwit CL. MRI compatibility and visibility assessment of implantable medical devices. J Magn Reson Imaging 1999; 9: 596-603.

[5] Khanicheh A, Muto A, Triantafyllou C, Weinberg B, Astrakas L, Tzika A, Mavroidis C. fMRI-compatible rehabilitation hand device. J NeuroEng Rehab 2006; 3: 24.

[6] Khanicheh A, Mintzopoulos D, Weinberg B, Tzika A, Mavroidis C. MR_CHIROD v.2: A fMRI compatible mechatronic hand rehabilitation device. In: Proceedings of the 10th IEEE International Conference on Rehabilitation Robotics; 2007.

[7] Flueckiger M, Bullo M, Chapuis D, Gassert R, Perriard Y. fMRI compatible haptic interface actuated with traveling wave ultrasonic motor. In: Proceedings of the 2005 Industry Applications Conference, 40th IAS Annual Meeting, Vol. 3; 2005: 2075–2082.

[8] Di Diodato L M, Mraz R, Baker S N, Graham S J. A Haptic Force Feedback Device for Virtual Reality-fMRI Experiments. IEEE Transactions on Neural Systems and Rehabilitation Engineering 2007; 15(4): 570–576.

[9] Yu N, Murr W, Blickenstorfer A, Kollias S, Riener R. An fMRI compatible haptic interface with pneumatic actuation. In: Proceedings of the 10th IEEE International Conference on Rehabilitation Robotics; 2007.

[10] Gassert R, Moser R, Burdet E, Bleuler H. MRI/fMRI-compatible robotic system with force feedback for interaction with human motion. IEEE/ASME Trans Mechatronics 2006; 11: 216–224.

[11] Gassert R, Dovat L, Lambercy O, Ruffieux Y, Chapuis D, Ganesh G, Burdet E, Bleuler H. A 2-DOF fMRI compatible haptic interface to investigate the neural control of arm movements. In: Proceedings of the 2006 IEEE International Conference on Robotics and Automation; 2006.

[12] Izawa J, Shimizu T, Aodai T, Kondo T, Gomi H, Toyama S, Ito K. MR compatible manipulandum with ultrasonic motor for fMRI studies. In: Proceedings of the 2006 IEEE International Conference on Robotics and Automation, Orlando; 2006.

[13] Mraz R, Hong J, Quintin G, Staines W R, McIlroy W E, Zakzanis K K, Graham S J. A Platform for Combining Virtual Reality Experiments with Functional Magnetic Resonance Imaging. CyberPsychology & Behavior 2003; 6(4): 359–368.

[14] Bardorfer A, Munih M, Zupan A, Primozic A. Upper Limb Motion Analysis Using Haptic Interface. IEEE/ASME TRANSACTIONS ON MECHATRONICS 2001; 6(3): 253–260.

[15] SPECIFICATIONS COMPARISON FOR THE PHANTOM PREMIUM 1.0, 1.5, 1.5 HIGH FORCE, AND 3.0 HAPTIC DEVICES http://www.sensable.com/products-datasheets.htm

[16] SIEMENS Medical Solutions, MAGNETIC RESONANCE MAGNETOM Trio A Tim System, Technical Drawing, 2006.

[17] NEMA Standards Publication MS 1-2001, Determination of Signal-to-Noise Ratio (SNR) in Diagnostic Magnetic Resonance Imaging.

[18] Friston KJ, Holmes AP, Worsley KJ, Poline JP, Frith CD, Frackowiak RSJ. Statistical parametric maps in functional imaging: a general linear approach. Human Brain Mapping 1995; 2: 189–210.

[19] Schaefers G. Testing MR Safety and Compatibility. Engineering in Medicine and Biology Magazine, IEEE; 27(3): 23–27.

[20] Chapman H, Gavrilescu M, Wang H, Kean M, Egan G, Castiello U. Posterior parietal cortex control of reach-to-grasp movements in humans. Eur J Neurosci 2002; 15: 2037–2042.

[21] Desmurget M, Gréa H, Grethe JS, Prablanc C, Alexander GE, Grafton ST. Functional anatomy of nonvisual feedback loops during reaching: a positron emission tomography study. J Neurosci 2001; 21: 2919–2929.

[22] Naranjo JR, Brovelli A, Longo R, Budai R, Kristeva R, Battaglini PP. EEG dynamics of the frontoparietal network during reaching preparation in humans. Neuroimage 2007; 34: 1673–1682.